Excellent Absorption of $LaCo_xO_3$ Over Full Solar Spectrum and Direct Photothermal Energy Storage of $Ca(OH)_2$–$LaCo_xO_3$

Lin Zhu, Rui-Min Hao, Chao-Yang Chang, and Qin-Pei Wu*

School of Chemistry and Chemical Engineering, Beijing Institute of Technology, Beijing, 102488, China

Abstract: Photothermal conversion is a vital way for solar energy applications. The strong absorption of near Infrared light is essential for excellent photothermal performance. In this study, we demonstrated that nano $LaCo_xO_3$ is able to harvest light intensely across the full solar spectrum with high photothermal temperature. A core-shell-like structure of $LaCo_xO_3$-coated $Ca(OH)_2$ particles was fabricated and shows excellent photothermal conversion, high kinetics of dehydration and remarkable cycle stability of heat storage and release. The photothermal dehydration-conversion of $Ca(OH)_2$ increases 8.4-fold. Results demonstrate the multifunctionality of $LaCo_xO_3$, intensifying light harvesting, high photothermal conversion, good stability, considerable strength, and porous framework favouring the performance of photothermal storage and release cycles. $LaCo_xO_3$–$Ca(OH)_2$ composite can simultaneously harvest light and store thermal energy.

Keywords: Cobalt, Hydroxide, Absorption, Photothermal energy, Solar, Thermal storage.

1. INTRODUCTION

The sun irradiation on the Earth is about 4.3 x 10^{13} GJ/h, which is nearly the whole energy consumption of the world in one year [1]. However, the usage of this huge renewable resource is limited by its intermittency and instability. Technology in thermal-energy storage is developed to overcome these issues [1, 2]. Molten salts have been largely used for heat storage in solar-thermal-power plant since the last century [3]. Basing on reversible thermochemical reaction, thermochemical heat storage (TCHS) technology provides a solution for long-term storage, *e.g*., storing the strong solar energy in the summer and then releasing in the winter [4, 5]. For instance, hydroxides and salt hydrates charge thermal energy via dehydration and discharge with the reverse hydration reaction [6, 7]. Carbonates conduct heat storage and release with pyrolysis and the reverse carbonation reaction, respectively [8, 9]. The TCHS conversion and kinetics dominate the efficiency of the thermal charge and discharge [10, 11]. Conventionally, solar-thermal-energy storage is performed through a continuous-multistep process, *i.e*., light harvesting and photothermal conversion by the corresponding materials, heat transfer with a fluid and tubes, and the heat stored with energy-storage materials in a heat exchanger [1, 3, 12]. This complicate process is expected to be substituted by a one-step system, direct solar-thermal conversion and thermal-energy storage; namely, photothermal storage (PTS), which leads to low cost, less equipment and concise procedure [1].

Ordinarily, thermal-energy-storage materials (TESM) absorb sunlight very weakly, which must be enhanced by absorbers to harvest light. Some metal oxides were employed to enhance the light absorption of $CaCO_3$ such as $FeMnO_3$–Fe_2O_3, oxide mixture of CuO–(CoO_x/CrO_x/FeO_x/MnO_x), SiC–MnO_2, FeO_x/Al_2O_3, MnO_x/Cr_2O_3, and co-doped Ce/Co/Mn oxide [13-18]. Besides the absorption, however, photothermal conversion, photothermal temperature, and the cyclo-stability of photothermal storage and heat releasing are also vital index to evaluate the performance of a direct photothermal-storage system.

It is reported that $LaCo_xO_3$ has metallic behavior via the semiconductor–metal transition occurring at 500 K [19]. Metals characterize high free carrier density, which supports surface plasmonic resonance (SPR) absorption conducive to high photothermal conversion [20-22]. Herein, we report that $LaCo_xO_3$ is able to harvest light efficiently over the full solar spectrum, which is also a multifunctional material to boost photothermal conversion, dehydration conversion and energy-charge-discharge reversibility of hydroxides.

2. EXPERIMENTAL

2.1. Chemicals and Instruments

All the chemicals employed, $Co(NO_3)_2{\cdot}6H_2O$, $La(NO_3)_3{\cdot}6H_2O$, polyethylene glycol, and glycine, were purchased from Beijing Chemical Co., Ltd., China. These chemicals were recrystallized before use. $Ca(OH)_2$ (98.8%) was prepared with a previous procedure.[6] Xe lamp (GME Xe-300F, 300–2500 nm) was employed to simulate solar irradiation. Differential scanning calorimetry (DSC) and thermogravimetric analysis (TG) were carried out with SDT–Q600. The

*Address correspondence to this author at the School of Chemistry and Chemical Engineering, Beijing Institute of Technology, Beijing, 102488, China; E-mail: qpwu@bit.edu.cn

E-ISSN: 2410-2199/23

optical absorption was recorded with a Shimadzu UV-3600 spectrophotometer (200–2500 nm). Pure $BaSO_4$ was used as the reflectance standard material.

The compositions and crystallographic phase of as-prepared materials were identified on an X-ray diffractometer (XRD, Ultima Ⅳ) with monochromatized Cu-K_α radiation (0.154059 nm, 40 kV). The XRD patterns were operated in the 2θ range of 10° to 80° at a scanning rate of 2° min^{-1}. Micromorphology of the materials was measured by scanning electron microscopy (SEM, ZEISS GeminiSEM 300) and transmission electron microscopy (TEM, JEOL JEM-F200) micrographs. X-ray photoelectron spectroscopy (XPS) spectra were recorded with the Thermo Scientific K-Alpha photoelectron spectrometer by using an Al K_α radiation source (1486.6 eV).

2.2. Preparation of $LaCo_xO_3$ and $Ca(OH)_2$–$LaCo_xO_3$ Composites

All the materials were prepared via nitrate pyrolysis. Preparation of lanthanum cobaltites with porous nanostructure: solution a: $Co(NO_3)_2{\cdot}6H_2O$ (1.31 g, 4.5 mmol) and $La(NO_3)_3{\cdot}6H_2O$ (1.95 g, 4.5 mmol) was dissolved in deionized water (10 mL) and followed by adding ethanol (5 mL). Solution b: glycine (0.75 g) was dissolved in a solution of deionized water–ethanol (20 mL, *v*/*v*=2:1). This solution was mixed with solution a and stirred at 80 ℃ to be a gel, which was sequentially maintained at 140 ℃ for 2 h, 280 ℃ for 4 h, and 650 ℃ for 4 h to form the desired nano $LaCo_xO_3$.

General procedure for preparation of core–shell-like $Ca(OH)_2$–$LaCo_xO_3$ composites: solution a: $Co(NO_3)_2{\cdot}6H_2O$ (0.58 g), glycine (0.5 g), and $La(NO_3)_3{\cdot}6H_2O$ (0.87 g) were dissolved in deionized water (10 mL) and followed by adding ethanol (5 mL). Solution b：polyethylene glycol (1 g) was dissolved in deionized water (5 mL) and mixed with solution a. This mixture is concentrated under reduced pressure to be viscose and followed by adding $Ca(OH)_2$ powder (2.17 g). After stirring for 10 min, the mixture was dried at 80 ℃. The solid was sequentially calcined at 180 ℃ for 4 h, 280 ℃ for 3 h, and 800 ℃ for 4 h to give CaO–$LaCo_xO_3$ composite. After cooled to room temperature, deionized water (2.0 mL) was added for hydrolyzation in 10 min, and then dried at 120 ℃ for 5 h to form $Ca(OH)_2$–18.45 wt% $LaCo_xO_3$ composite with a core–shell-like structure.

3. RESULTS AND DISCUSSION

3.1. Photothermal Performance of Nano $LaCo_xO_3$ and $Ca(OH)_2$–$LaCo_xO_3$ Composite

The optimal absorption of nano $LaCo_xO_3$ was measured and shown in Figure **1a**. A very strong absorption curve was clearly observed across full solar wavelength and the absorbance is much stronger than that of Co_3O_4. The photothermal performance of nano $LaCo_xO_3$ was further evaluated by the photothermal temperature (T_p) under Xe-lamp irradiation. Figure **1b** indicates that the T_p rises sharply under irradiation with various intensity of light, namely, the different electric current of the lamp, 16 A, 18 A, and 20 A. Under the first 30-s irradiation, almost all the T_ps rise up to the maxima and increase with the current's increase. The maximum T_ps are 780±2 °C, 731±2 °C, and 669±3 °C for nano $LaCo_xO_3$ at 20 A, 18 A, and 16 A, respectively. In comparison, under similar conditions, the maximum T_ps shown by Co_3O_4 are only 653±2 °C, 589±2 °C, and 539±1 °C, respectively.

To evaluate the capacity of nano $LaCo_xO_3$ in enhancing the absorption of $Ca(OH)_2$, a core–shell-like structure of $LaCo_xO_3$-coated $Ca(OH)_2$ composites was constructed for both the photothermal efficiency and the energy density stored in $Ca(OH)_2$. The amount of $LaCo_xO_3$ in this composite was briefly optimized. A number of composites of $Ca(OH)_2$–$LaCo_xO_3$ with different contents of $LaCo_xO_3$, 7.0 wt%, 18.5 wt%, and 24.0 wt% were fabricated and termed as CaCoLa-y, the y is the number of mass percentage, *i.e.*, 7, 18, and 24, respectively. The T_p of these composites was measured under Xe-lamp irradiation (18 A). As shown in Figure **1c**, all T_ps rise also quickly up to the highest number in ca 30 s, namely, 693±2 °C, 724±4 °C, and 736±3 °C for CaCoLa-7, CaCoLa-18, and CaCoLa-24, respectively. The much lower T_p showed by CaCoLa-7 indicated that 7 wt% of $LaCo_xO_3$ is not enough to surround the full surface of $Ca(OH)_2$ particles, leading to low photothermal efficiency. The similar T_ps' numbers showed by both CaCoLa-18 and CaCoLa-24 may elucidate that ca 18 wt% of $LaCo_xO_3$ is nearly perfect to cover the surface of the $Ca(OH)_2$ powders. Thus, CaCoLa-18 composite was selected as a candidate for further investigation. Under similar conditions, the bare $Ca(OH)_2$ powders showed only 466.5±2.5 °C.

Moreover, the dehydration conversion (α) under irradiation is another key index to the efficiency of photothermal conversion for this composite. The α was calculated using Equation 1. Under irradiation, milligram samples of CaCoLa-18 were collected at some intervals for TG analysis to examine mass losses (m_t). Under 30-min irradiation, the α values are 77.2 wt%, 87.4 wt%, and 95.4 wt% corresponding to the

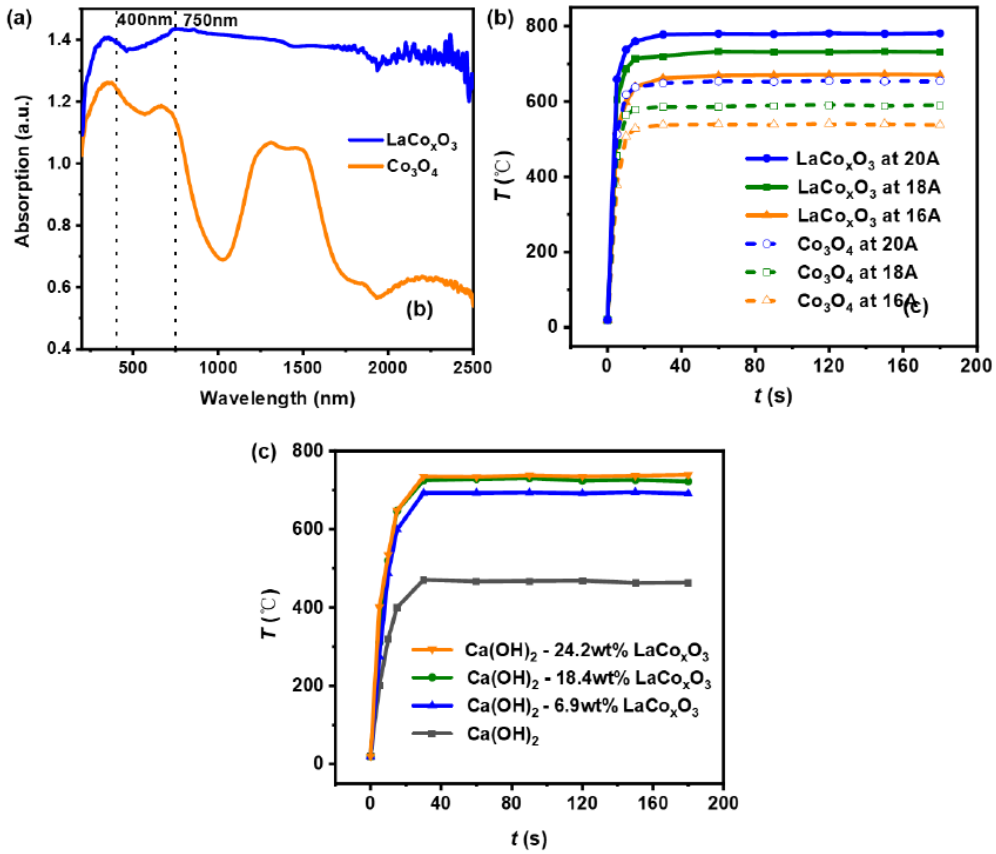

Figure 1: (**a**) Absorption curves of $LaCo_xO_3$ and Co_3O_4. (**b**) photothermal temperature of $LaCo_xO_3$ and Co_3O_4 under irradiation of Xe–lamp. (**c**) photothermal temperature of $Ca(OH)_2$–x% $LaCo_xO_3$ composite under Xe lamp.

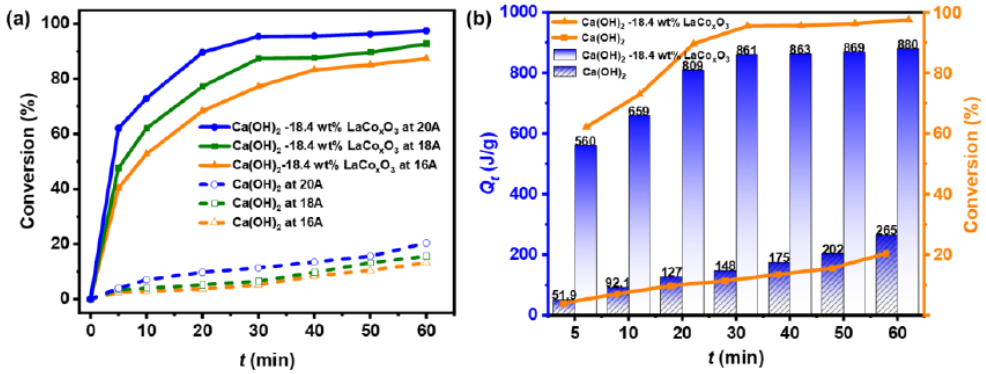

Figure 2: (**a**) Relations between dehydration conversion (α) and irradiation time (min) for $Ca(OH)_2$-18.4 wt% $LaCo_xO_3$ and mere $Ca(OH)_2$ under different irradiation. (**b**) relations of dehydration conversion (α) and heat amount with irradiation time (min) for $Ca(OH)_2$-18.4 wt% $LaCo_xO_3$ and mere $Ca(OH)_2$ under light (20 A).

lamp-current of 16 A, 18 A, and 20 A, respectively (Figure **2a**). In contrast, under similar conditions, the α values of pure $Ca(OH)_2$ are only 5.2 wt%, 6.6 wt%, and 11.4 wt%, respectively. Thus, these data show that the α is pronouncedly improved by nano $LaCo_xO_3$ particles and an 8.4-fold increase is achieved. Further, after 60-min irradiation, the α values of CaCoLa-18 rise to be 87.4 wt%, 92.7 wt%, and 97.5 wt% in the increase intensity of light. Therefore, 60-min irradiation is nearly enough for CaCoLa-18 to complete heat storage (α =97.5 wt%). Nano $LaCo_xO_3$ is able to boost the light harvesting, photothermal conversion, and heat storage of $Ca(OH)_2$ in one-step.

$$\alpha_t = 1 - \frac{m_t}{m_o} \quad (1)$$

$$Q_t = \alpha_t \times Q_0 \quad (2)$$

$$V_Q = Q_t / t \quad (3)$$

Table 1: Thermal-Storage Rate for $Ca(OH)_2$–$LaCo_xO_3$ and $Ca(OH)_2$

t/min	-	5	10	20	30	40	50	60
V_Q/(J/g•min)	$Ca(OH)_2$	10.4	9.2	6.3	4.9	4.4	4.0	4.4
	CaCoLa-18	112	65.9	40.4	28.7	21.6	17.4	14.7

where m_t is the mass percentage loss of the composite showed by TG after a *t*-min irradiation, m_0 represents the initial mass percentage loss of the composite, Q_0 is the maximum amount of stored-heat in $Ca(OH)_2$–$LaCo_xO_3$, and Q_t represents the amount of stored heat under a *t*-min irradiation.

Furthermore, The amount of stored heat (Q_t) under irradiation for CaCoLa-18 and $Ca(OH)_2$ was derived from Equation 2 and depicted in Figure **2b**. The composite exhibited a stored heat of 861 J/g in 30-min irradiation, which is approximately 5.8 times higher than that stored in bare $Ca(OH)_2$ (148 J/g). Over a 60-min irradiation, the Q_t values for CaCoLa-18 and bare $Ca(OH)_2$ are 880 and 265 J/g, respectively. The photothermal-storage rate (v_Q) was calculated using equation 3 (Table **1**). In the first 30-min irradiation, the v_Q values are 28.7 and 4.9 J/g•min for CaCoLa-18 and bare $Ca(OH)_2$, respectively, which is 5.86-fold increase. Thus, nano $LaCo_xO_3$ is also capable to improve strongly the photothermal-storage kinetics of $Ca(OH)_2$.

3.3. Photothermal Charge-Discharge Cycles

The stability of the dehydration–hydration cycle is much weak for pure $Ca(OH)_2$ mainly due to the poor permeability induced by agglomeration during this process [23]. The reversibility of heat charge and discharge for $Ca(OH)_2$–$LaCo_xO_3$ was investigated under Xe-lamp irradiation. Based on the nearly thorough dehydration of CaCoLa-18 under 60-min irradiation (Figure **2a**), a 60-min irradiation was conducted for the heat charge of this composite. After cooling to around 50°C, deionized water was added for hydrolyzation to release the heat completely. Thus, one cycle of heat storage and release was completed. This photothermal cycle was repeated 30 times. After every five cycles, samples (ca 5 mg) were collected from the dehydration product for TG analysis. The photothermal α is calculated in terms of Equation 1. The variation of α with the number of cycles is depicted in Figure **3a**. After 30 cycles, the α is still excellent (81.4%). In contrast, the α value for bare $Ca(OH)_2$ is only 2.8% after 30 cycles under similar charge–discharge conditions. Hence, $LaCo_xO_3$ tremendously raises the reversibility, which is resulted from the brilliant structure-stability with high porosity.

3.4. X-ray Diffraction and X-Ray Photoelectron Analysis

The crystal phase and the composition of the as-prepared $LaCo_xO_3$ were verified by X-ray diffraction (XRD) technology. Figure **3b** shows that the XRD pattern matches well with the JCPD standard cubic $LaCo_xO_3$ (No 75–0279) with a high purity [24]. The main diffraction peaks, at 2θ, 23.266°, 33.138°, 40.884°, 47.568°, 59.198°, and 69.547°, correspond well to the crystalline planes (100), (110), (111), (200), (211), and (220), respectively. The lattice parameters, a=b=c=3.84 Å, $\alpha=\beta=\gamma=90$ °, were derived from the XRD data, which are consistent with standard data of the

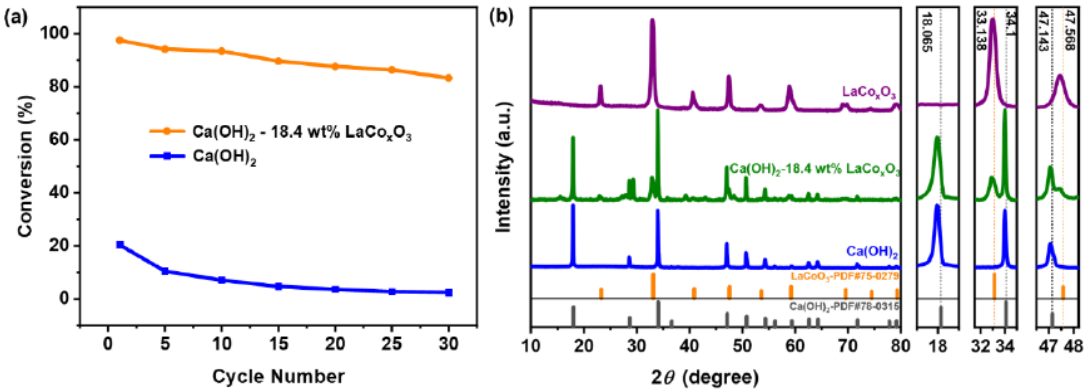

Figure 3: (**a**) Relation between dehydration–conversion and cyclic numbers for $Ca(OH)_2$ and $Ca(OH)_2$–18.4 wt% $LaCo_xO_3$ composite. (**b**) X-ray diffractometry patterns of the as-prepared $LaCo_xO_3$, $LaCo_xO_3$-$Ca(OH)_2$ and $Ca(OH)_2$.

cubic phase. Moreover, the remarkable broad bands indicate the existence of many lattice defects or oxygen vacancies. For the core-shell-like $Ca(OH)_2$–$LaCo_xO_3$ composite, the main diffraction peaks also demonstrate well the existence of both $Ca(OH)_2$ and cubic crystalline $LaCo_xO_3$ species.

The chemical nature of as-prepared $LaCo_xO_3$ and CaCoLa-18 was accurately confirmed using XPS analysis. The elemental survey spectrum clearly exhibits the presence of lanthanum, cobalt, calcium and oxygen elements (Figure **4a**). The O 1s spectra were deconvoluted into three peaks, 528.04, 530.59, and 532.48 eV. The first is attributed to the crystal-lattice oxygen ions of Co-O. The second peak corresponds to the absorbed oxygen species (O_2^{2-}, O_2^-, and O^-) resulted from oxygen vacancies (Figure **4b**) [24-26]. This result is consistent with the data of the relative XRD analysis shown in Figure **3b**.

The La 3d spectra of $LaCo_xO_3$ were deconvoluted into two doublet peaks at 833.63/837.28 eV and

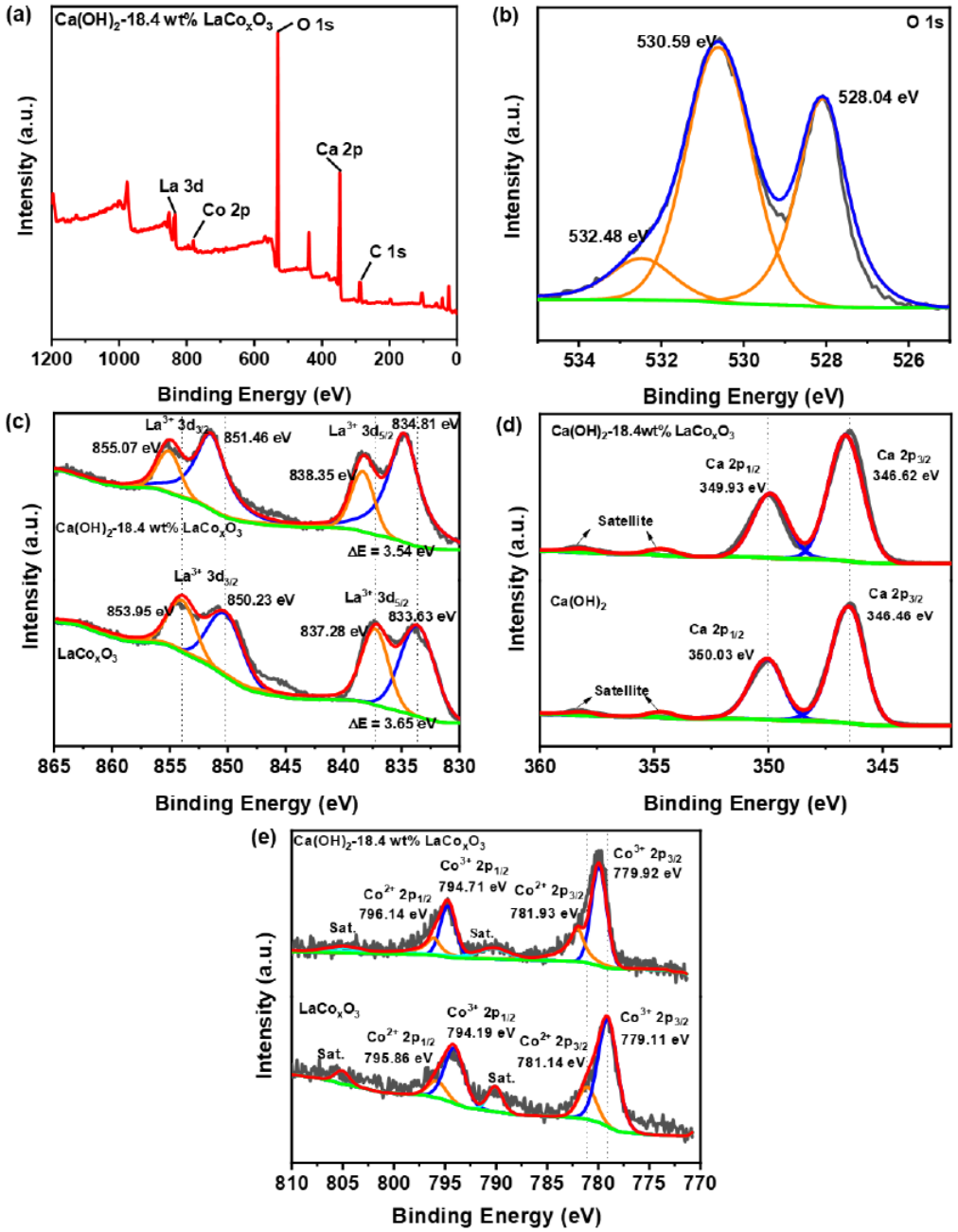

Figure 4: X-ray photoelectron spectroscopy spectra. (**a**) elemental survey spectrum of $Ca(OH)_2$–$LaCo_xO_3$. (**b**) deconvoluted spectrum of O 1s for $LaCo_xO_3$. (**c**) deconvoluted spectrum of La 3d for $LaCo_xO_3$ and $Ca(OH)_2$–$LaCo_xO_3$. (**d**) deconvoluted spectrum of Co 2p for $LaCo_xO_3$ and $Ca(OH)_2$–$LaCo_xO_3$.

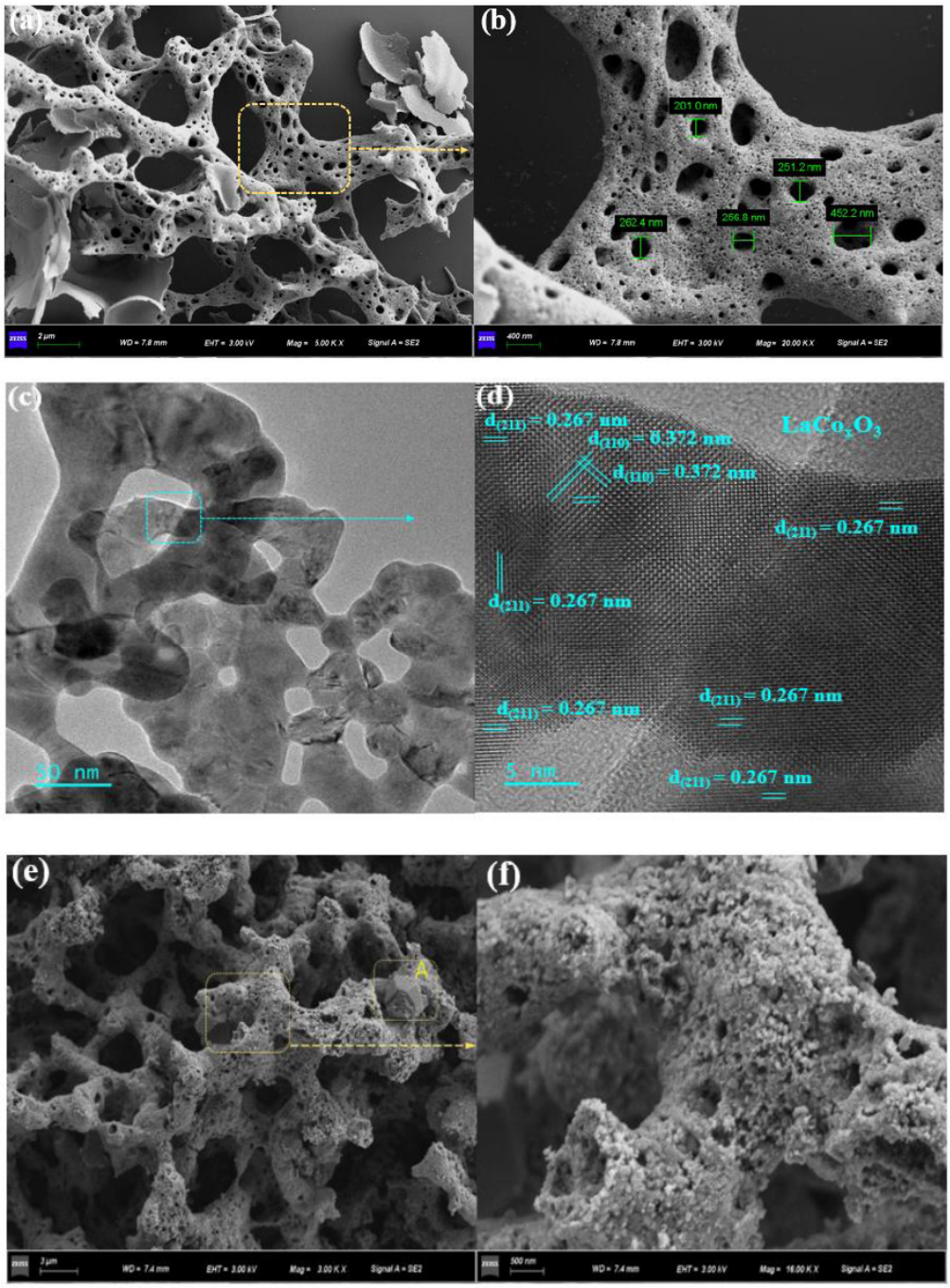

Figure 5: (**a**) and (**b**) SEM images for as-prepared $LaCo_xO_3$. (**c**) and (**d**) TEM and HRTEM micromorphology of $LaCo_xO_3$. (**e**) and (**f**) SEM images of $Ca(OH)_2$–$LaCo_xO_3$ (A area shows a particle of $Ca(OH)_2$).

850.23/853.95 eV, corresponding to La $3d_{5/2}$ and La $3d_{3/2}$ spin-states, respectively. These peaks confirm the presence of La^{3+} state and reflects the charge transfer between O2p and La4f orbits in La-O (Figure **4c**) [27]. For the $Ca(OH)_2$–18.5 wt% $LaCo_xO_3$ composite, the deconvoluted spectra of La 3d show similar pattern with four peaks and these peaks remarkablely shift to higher BEs clearly, indicating the strong interaction with $Ca(OH)_2$. The deconvoluted Ca 2p spectra of the $Ca(OH)_2$–$LaCo_xO_3$ is similar to that of pure $Ca(OH)_2$. Two specific peaks shift slightly to high binding energy, also confirming the interaction between $Ca(OH)_2$ and $LaCo_xO_3$. This interaction promotes the dehydration conversion and improves the heat storage kinetics.

In the deconvoluted Co2p spectra (Figure **4d**), two prominent peaks are observed at 779.24 and 794.33 eV, corresponding to the Co^{3+} 2p3/2 and 2p1/2 spin–orbit states in CoO_3^{3-} species, respectively. This BE splitting of Co $2p_{3/2}$–Co $2p_{1/2}$ (15.2 eV) is also

consistent well with the literature data for $LaCoO_3$ [27, 28]. The satellite peaks center at ~789.5 and 804.84 eV indicates the presence of paramagnetic Co^{2+} at the surface. The weak peaks at 781.1 and 795.9 eV also correspond to Co^{2+} 2p3/2 and Co^{2+}2p1/2 spin–orbit states. The peak-area ratio of Co^{2+} 2p3/2 to Co^{3+} 2p3/2 is 0.36 [24]. Compared to the Co2p spectra of $LaCo_xO_3$, all these BE peaks for CaCoLa-18 shift upward and the peak-area ratio of Co^{2+} 2p3/2 to Co^{3+} 2p3/2 increases by 0.56. These results indicate the occurrence of Co^{2+} in the as-prepared $LaCo_xO_3$ material. Co^{2+} is Jahn-Teller active and induces lattice defects and oxygen vacancies (Vo). More concentration of Co^{2+} generates large Vo, conducive to increasing free carrier density and inducing semiconductor–metal transfer. This may elucidate the strong absorption of $LaCo_xO_3$ across the entire solar wavelength (Figure **2a**) [19, 31].

The surface micromorphology of the as-prepared $LaCo_xO_3$ was identified by scanning electron microscope (SEM, Figure **5**(**a**) and (**b**)). A porous foam-like framework with numerous nano-size pores was observed to this cobaltite material [30]. This nano structure is favorable to solar absorption and increases the photo-thermal conversion efficiency [20, 32, 33].

Transmission electron microscopy (TEM) micrographs of $LaCo_xO_3$ presented in Figure **5c** confirm also the porous structure of $LaCo_xO_3$. The high-resolution TEM images show clear crystalline fringes (Figure **5d**). The facet spacings of 0.267, 0.216, 0.219, and 0.372 nm correspond well to the nano crystal plane of (211), (222), (220), and (110) in cubic $LaCo_xO_3$, respectively. These crystalline facets also correspond to the relative diffraction peaks at 2θ =33.138^o and 59.198^o in the relative XRD spectrum (Figure **2**).

Additionally, Figure **5e** and **5f** indicate that a core–shell-like structure of the as-prepared $Ca(OH)_2$–$LaCo_xO_3$ composite was well formed and the shell possesses abundant nanopores to form a framework structure, which favors mass transfer and deagglomeration [34, 35]. Thus, the nano structure of $LaCo_xO_3$ benefits light harvesting, the photothermal conversion and the kinetics of $Ca(OH)_2$ dehydration.

4. CONCLUSIONS

We demonstrated that $LaCo_xO_3$ nanoparticles can exceptionally absorb sunlight over the whole solar wavelength, which also considerably enhances the absorption, photothermal temperature, and dehydration conversion of $Ca(OH)_2$. The core–shell-like $LaCo_xO_3$–$Ca(OH)_2$ composite exhibits excellent capability of high photothermal conversion, brilliant dehydration kinetics, and good reversibility in photothermal charge–discharge cycles. This composite is a potential candidate for performing photothermal conversion and energy storage in one step. Moreover, a porous framework of $LaCo_xO_3$ nano structure with good stability and high strength is also promising for solar steam generation, desalination, and photothermal reaction.

CONFLICTS OF INTEREST

The authors declare no conflict of interest.

REFERENCES

[1] A.J. Carrillo, J. Gonzalez-Aguilar, M. Romero, J.M. Coronado, Solar Energy on Demand: A review on high temperature thermochemical heat storage systems and materials, Chemical Reviews, 119 (2019) 4777-4816. https://doi.org/10.1021/acs.chemrev.8b00315

[2] S. Koohi-Fayegh, M.A. Rosen, A review of energy storage types, applications and recent developments, Journal of Energy Storage, 27 (2020) 101047 https://doi.org/10.1016/j.est.2019.101047

[3] E. Gonzalez-Roubaud, D. Perez-Osorio, C. Prieto, Review of commercial thermal energy storage in concentrated solar power plants: Steam vs. molten salts, Renewable & Sustainable Energy Reviews, 80 (2017) 133-148. https://doi.org/10.1016/J.RSER.2017.05.084

[4] P.E.S. Jimenez, A. Perejon, M.B. Guerrero, J.M. Valverde, C. Ortiz, L.A.P. Maqueda, High-performance and low-cost macroporous calcium oxide based materials for thermochemical energy storage in concentrated solar power plants, Applied Energy, 235 (2019) 543-552. https://doi.org/10.1016/j.apenergy.2018.10.131

[5] R. Bravo, C. Ortiz, R. Chacartegui, D. Friedrich, Hybrid solar power plant with thermochemical energy storage: A multi-objective operational optimisation, Energy Conversion and Management, 205 (2020) 112421. https://doi.org/10.1016/j.enconman.2019.112421

[6] Y.T. Li, M.T. Li, Z.B. Xu, Z.H. Meng, Q.P. Wu, Dehydration kinetics and thermodynamics of $ZrO(NO_3)_2$-doped $Ca(OH)_2$ for chemical heat storage, Chemical Engineering Journal, 399 (2020) 125841. https://doi.org/10.1016/j.enconman.2019.112421

[7] A. Fopah-Lele, J.G. Tamba, A review on the use of $SrBr_2 \cdot 6H_2O$ as a potential material for low temperature energy storage systems and building applications, Solar Energy Materials and Solar Cells, 164 (2017) 175-187. https://doi.org/10.1016/j.solmat.2017.02.018

[8] C. Ortiz, J.M. Valverde, R. Chacartegui, L.A. Perez-Maqueda, P. Gimenez, The Calcium-Looping ($CaCO_3$/CaO) process for thermochemical energy storage in Concentrating Solar Power plants, Renewable & Sustainable Energy Reviews, 113 (2019) 109252. https://doi.org/10.1016/j.rser.2019.109252

[9] M.T. Dunstan, F. Donat, A.H. Bork, C.P. Grey, C.R. Mueller, CO_2 capture at medium to high temperature using solid oxide-based sorbents: Fundamental Aspects, Mechanistic

Insights, and Recent Advances, Chemical Reviews, 121 (2021) 12681-12745.
https://pubs.acs.org/doi/10.1021/acs.chemrev.1c00100

[10] M.-T. Li, Y.-T. Li, L. Sun, Z.-B. Xu, Y. Zhao, Z.-H. Meng, Q.-P. Wu, Tremendous enhancement of heat storage efficiency for Mg $(OH)_2$-MgO-H_2O thermochemical system with addition of $Ce(NO_3)_3$ and LiOH, Nano Energy, 81 (2021) 105603.
https://doi.org/10.1016/j.nanoen.2020.105603

[11] S. Li, J. Liu, T. Tan, J. Nie, H. Zhang, Optimization of $LiNO_3$-$Mg(OH)_2$ composites as thermo-chemical energy storage materials, Journal of Environmental Management, 262 (2020) 110258.
https://doi.org/10.1016/j.jenvman.2020.110258

[12] M. Liu, N.H.S. Tay, S. Bell, M. Belusko, R. Jacob, G. Will, W. Saman, F. Bruno, Review on concentrating solar power plants and new developments in high temperature thermal energy storage technologies, Renewable & Sustainable Energy Reviews, 53 (2016) 1411-1432.
https://doi.org/10.1016/j.rser.2015.09.026

[13] Y. Da, Y. Xuan, L. Teng, K. Zhang, X. Liu, Y. Ding, Calcium-based composites for direct solar-thermal conversion and thermochemical energy storage, Chemical Engineering Journal, 382 (2020) 122815.
https://doi.org/10.1016/j.cej.2019.122815

[14] H.B. Zheng, C. Song, C. Bao, X.L. Liu, Y.M. Xuan, Y.L. Li, Y.L. Ding, Dark calcium carbonate particles for simultaneous full-spectrum solar thermal conversion and large-capacity thermochemical energy storage, Solar Energy Materials and Solar Cells, 207 (2020) 110364.
https://doi.org/10.1016/j.solmat.2019.110364

[15] B. Li, Y. Li, Y. Dou, Y. Wang, J. Zhao, T. Wang, SiC/Mn co-doped CaO pellets with enhanced optical and thermal properties for calcium looping thermochemical heat storage, Chemical Engineering Journal, 423 (2021) 130305.
https://doi.org/10.1016/j.cej.2021.130305

[16] C. Song, X.L. Liu, H.B. Zheng, C. Bao, L. Teng, Y. Da, F. Jiang, C. Li, Y.L. Li, Y.M. Xuan, Y.L. Ding, Decomposition kinetics of Al- and Fe-doped calcium carbonate particles with improved solar absorbance and cycle stability, Chemical Engineering Journal, 406 (2021) 126282.
https://doi.org/10.1016/j.cej.2020.126282

[17] Y. Da, J.L. Zhou, F.D. Zeng, Calcium-based composites directly irradiated by solar spectrum for thermochemical energy storage, Chemical Engineering Journal, 456 (2023) 140986.
https://doi.org/10.1016/j.cej.2022.140986

[18] Y. Da, J.L. Zhou, Multi-doping strategy modified calcium-based materials for improving the performance of direct solar-driven calcium looping thermochemical energy storage, Solar Energy Materials and Solar Cells, 238 (2022) 111613.
https://doi.org/10.1016/j.solmat.2022.111613

[19] A. Laref, S. Laref, S. Bin-Omran, Electronic structure, X-ray absorption, and optical spectroscopy of $LaCo_xO_3$ in the ground-state and excited-states, Journal of Computational Chemistry, 33 (2012) 673-684.
https://doi.org/10.1002/jcc.22896

[20] J. Li, W. Zhang, W. Ji, J. Wang, N. Wang, W. Wu, Q. Wu, X. Hou, W. Hu, L. Li, Near infrared photothermal conversion materials: mechanism, preparation, and photothermal cancer therapy applications, Journal of Materials Chemistry B, 9 (2021) 7909-7926.
https://doi.org/10.1039/d1tb01310f

[21] J. Li, Y. Zhang, Y. Huang, B. Luo, L. Jing, D. Jing, Noble-metal free plasmonic nanomaterials for enhanced photocatalytic applications-A review, Nano Research, 12 (2022) 10268-10291.
https://doi.org/10.1007/s12274-022-4700-0

[22] T.A. Wani, P. Garg, S. Bera, S. Bhattacharya, S. Dutta, H. Kumar, A. Bera, Narrow-Bandgap $LaMO_3$ (M = Ni, Co) nanomaterials for efficient interfacial solar steam generation, Journal of Colloid and Interface Science, 612 (2022) 203-212.
https://doi.org/10.1016/j.jcis.2021.12.158

[23] M. Xu, X. Huai, J. Cai, Agglomeration behavior of calcium hydroxide/calcium oxide as thermochemical heat storage material: A reactive molecular dynamics study, Journal of Physical Chemistry C, 121 (2017) 3025-3033.
https://doi.org/10.1021/acs.jpcc.6b08615

[24] T. Wu, X. Li, C.-H. Weng, F. Ding, F. Tan, R. Duan, Highly efficient $LaMO_3$ (M = Co, Fe) perovskites catalyzed Fentons reaction for degradation of direct blue 86, Environmental Research, 227 (2023) 115756.
https://doi.org/10.1016/j.envres.2023.115756

[25] J.T. Kloprogge, L.V. Duong, B.J. Wood, R.L. Frost, XPS study of the major minerals in bauxite: Gibbsite, bayerite and (pseudo-) boehmite, Journal of Colloid and Interface Science, 296 (2006) 572-576.
https://doi.org/10.1016/j.jcis.2005.09.054

[26] H. Guo, X. Kou, Y. Zhao, S. Wang, Q. Sun, X. Ma, Effect of synergistic interaction between Ce and Mn on the CO_2 capture of calcium-based sorbent: Textural properties, electron donation, and oxygen vacancy, Chemical Engineering Journal, 334 (2018) 237--246.
https://doi.org/10.1016/j.cej.2017.09.198

[27] S. Jayapandi, P. Soundarrajan, S.S. Kumar, D. Lakshmi, M.D. Albaqami, M. Ouladsmane, G. Mani, Efficient Z-scheme $LaCo_xO_3/In_2O_3$ heterostructure photocatalyst for fast dye degradation under visible light irradiation, Research on Chemical Intermediates, 48 (2022) 4419-4442.
https://doi.org/10.1007/s11164-022-04832-4

[28] S. Ben Hammouda, F. Zhao, Z. Safaei, V. Srivastava, D.L. Ramasamy, S. Iftekhar, S. Kalliola, M. Sillanpaa, Degradation and mineralization of phenol in aqueous medium by heterogeneous monopersulfate activation on nanostructured cobalt based-perovskite catalysts $ACoO_3$ (A = La, Ba, Sr and Ce): Characterization, kinetics and mechanism study, Applied Catalysis B-Environmental, 215 (2017) 60-73.
https://doi.org/10.1016/j.apcatb.2017.05.051

[29] N. Orlovskaya, D. Steinmetz, S. Yarmolenko, D. Pai, J. Sankar, J. Goodenough, Detection of temperature- and stress-induced modifications of $LaCoO_3$ by micro-Raman spectroscopy - art. no. 014122, Physical Review B, 72 (2005) 014122.
http://dx.doi.org/10.1103/PhysRevB.72.014122

[30] M.M. Natile, E. Ugel, C. Maccato, A. Glisenti, LaCoxO3: Effect of synthesis conditions on properties and reactivity, Applied Catalysis B: Environmental, 72 (2007) 351-362.
https://doi.org/10.1016/j.apcatb.2006.11.011

[31] X.M. Cui, Q.F. Ruan, X.L. Zhu, X.Y. Xia, J.T. Hu, R.F. Fu, Y. Li, J.F. Wang, H.X. Xu, Photothermal nanomaterials: A powerful light-to-heat converter, Chemical Reviews, 123 (2023) 6891-6952.
https://doi.org/10.1021/acs.chemrev.3c00159

[32] J. Lu, J. Wu, W. Xu, H. Cheng, X. Qi, Q. Li, Y. Zhang, Y. Guan, Y. Ling, Z. Zhang, Room temperature synthesis of tetragonal BiOI photocatalyst with surface heterojunction between (001) facets and (110) facets, Materials Letters, 219 (2018) 260-264.
https://doi.org/10.1016/j.matlet.2018.01.175

[33] J.U. Kim, S. Lee, S.J. Kang, T.-i. Kim, Materials and design of nanostructured broadband light absorbers for advanced light-to-heat conversion, Nanoscale, 10 (2018) 21555-21574.
https://doi.org/10.1039/c8nr06024j

[34] Y. Liu, J. Zhao, S. Zhang, D. Li, X. Zhang, Q. Zhao, B. Xing, Advances and challenges of broadband solar absorbers for efficient solar steam generation, Environmental Science-Nano, 9 (2022) 2264-2296.
https://doi.org/10.1039/D2EN00070A

[35] M. Hartmann, M. Thommes, W. Schwieger, Hierarchically-ordered zeolites: A critical assessment, Advanced Materials Interfaces, 8 (2021) 2001841. https://doi.org/10.1002/admi.202001841

Received on 04-12-2023 Accepted on 26-12-2023 Published on 31-12-2023

DOI: https://doi.org/10.31875/2410-2199.2023.10.09